The Pennsylvania State University

The Graduate School

LOW-FIELD ELECTRICALLY DETECTED MAGNETIC RESONANCE AND NEAR-ZERO FIELD MAGNETORESISTANCE IN AMORPHOUS HYDROGENATED SILICON

A Thesis in

Engineering Science and Mechanics

by

Noah Brous

Submitted in Partial Fulfillment
of the Requirements
for the Degree of

Master of Science

August 2020

The thesis of Noah Brous was reviewed and approved by the following:

Patrick M. Lenahan
Distinguished Professor of Engineering Science and Mechanics
Thesis Advisor

Saptarshi Das
Assistant Professor of Engineering Science and Mechanics

Sahin K. Ozdemir
Associate Professor of Engineering Science and Mechanics

Judith Todd
Department Head of Engineering Science and Mechanics
P.B. Breneman Chair
Professor of Engineering Science and Mechanics

ABSTRACT

The goal of this work is to study defect centers in amorphous hydrogenated silicon (a-Si:H) using both electrically detected magnetic resonance (EDMR) and near zero-field magnetoresistance (NZFMR) to establish an understanding of the physical connection between EDMR and NZFMR. Numerous EDMR and NZFMR traces taken at varying bias across an a-Si:H sample are compared. Through comparisons of NZFMR and EDMR, it was determined that NZFMR has a somewhat similar response to EDMR in a-Si:H. An EDMR half field signal, the result of forbidden dipolar interactions, is observed in this work. One can determine the approximate distance between defects from the half field response. The average defect distance (r_d) and defect density ($1/{r_d}^3$) were roughly calculated to be approximately 57 Angstroms and about $5.4\text{x}10^{18}\text{cm}^{-3}$.

TABLE OF CONTENTS

List of Figures v

List of Tables vi

Chapter 1 Amorphous Hydrogenated Si (a-Si:H) 1

Chapter 2 Theory and Experimental Design 2

Electron Paramagnetic Resonance 2
Electrically Detected Magnetoresistance and Mode of Transport 4
Near Zero Field Magneto Resistance 8
Experimental Design 10

Chapter 3 Results 13

Chapter 4 Analysis and Conclusions 15

References 19

LIST OF FIGURES

Figure 1: Zeeman splitting versus magnetic field....2

Figure 2: a) pictorial representation of a triplet state. b) pictorial representation of a singlet state [13,14]....5

Figure 3: Energy diagram, depicting the allowed transitions between the four possible states of the coupled defects [8]....7

Figure 4: Low-Field apparatus for EDMR and NZFMR measurements [8]....11

Figure 5: EDMR/NZFMR traces at varying bias in a-Si:H....13

Figure 6: NZFMR traces at varying bias of a-Si:H....14

Figure 7: Amplitude the NZFMR response with the RF on, RF off and EDMR....15

Figure 8: Results of Magnetoresistance and Magnetic Resonance amplitudes vs. bias in a-SiN:H devices [12]....16

LIST OF TABLES

Table 1: List of constant parameters during EDMR and NZFMR experiments 11

Chapter 1

Amorphous Hydrogenated Si (a-Si:H)

Amorphous silicon, a-Si, is an excellent "model system" for novel spin related techniques. a-Si has a controllable density of well understood dangling bonds [1]. A technological advantage of a-Si is that it can be deposited at relatively low temperatures [2,3]. When processing a-Si, hydrogen can be included to consume most of the dangling bonds [3]. This process will form amorphous hydrogenated silicon or a-Si:H. a-Si:H has been used in solar cells, thin film transistors, nanocones, waveguides, nanowires, and as a buffer layer [2,4,5].

More recently, Silicon-on-insulator (SOI) waveguides consisting of an a-Si:H core have been utilized because the low deposition temperature minimizes the risk of damaging the surrounding material [2]. Waveguides are used to transport sound or electromagnetic radiation [2]. In the case of solar cells, it is important to understand that dangling bonds will decrease the conversion efficiency [6]. a-Si is useful for this application since hydrogen can be implemented to passivate dangling bonds [6]. Another use for intrinsic a-Si:H is as a buffer layer between the doped a-Si:H and c-Si in a heterostructure solar cell [4]. a-Si:H is deposited on crystalline silicon to form a heterojunction. Then the a-Si:H is doped to the desired parameters. a-Si:H is intentionally doped to leave a few nanometers of a-Si:H undoped in between the doped region and the crystalline Si [4]. The purpose of this intrinsic layer is to increase the energy conversion efficiencies [4]. a-Si is thus useful across a wide range of applications in materials science.

Chapter 2

Theory and Experimental Design

Electron Paramagnetic Resonance

Electron paramagnetic resonance (EPR) is a powerful analytical tool to study defects in semiconductors and is the foundation for understanding electrically detected magnetic resonance (EDMR). The following is a brief and simplified discussion of EPR. EPR is conducted by exposing a semiconductor to a slowly varying magnetic field, B, and microwave radiation perpendicular to the magnetic field with a frequency of υ. The detection scheme in EPR involves measurements of the absorption of the microwave radiation [7]. When a semiconductor with paramagnetic defects is exposed to a large magnetic field, Zeeman splitting will cause a separation of electron spin energy levels between $m_s = +1/2$ and $m_s = -1/2$. Each spin will either align with the applied magnetic field or oppose it, hence splitting the electrons into two energy groups as shown below in figure 1.

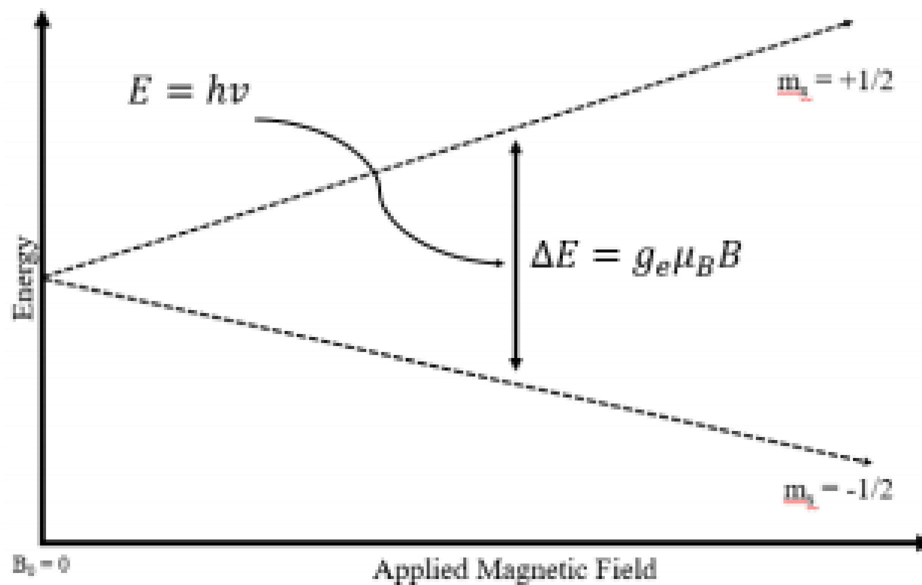

Figure 1: Zeeman splitting versus magnetic field

If Planck's constant, h, times the microwave frequency, υ, is equal to the energy difference between +1/2 and -1/2 spin states, the electron spins may flip. This corresponding field frequency combination is called the resonance condition. In the simplest possible case, where the unpaired electron spins are otherwise unperturbed by the environment except by the applied field and microwave radiation, the resonance condition is

$$\Delta E = h\nu = g_e \mu_e B \quad (1)$$

where g_e is the Landé g factor, 2.0023…, μ_e is the Bohr magneton, and ΔE is the difference between the energy levels (+1/2 and -1/2). The local magnetic field experienced by the electron can be described by two interactions: spin-orbit coupling, and electron-nuclear hyperfine interactions. Spin-orbit coupling involves the orbital angular momentum of the electron with respect to the nucleus, and electron nuclear hyperfine interactions are the interactions between the electron's magnetic moment and that of magnetic nuclei [8]. Spin-orbit coupling can be accounted for by replacing the Landé g factor with an orientation dependent g-factor, $\boldsymbol{g}$, generally expressed as a second rank tensor. Electron-nuclear hyperfine interactions can be accounted for by inserting an additional term to Eq. (1). For the case of a single electron interacting with a single nucleus [8]

$$\Delta E = h\nu = \boldsymbol{g} \mu_e B + \mu_I A \quad (1.1)$$

where μ_I is the nuclear spin quantum number and A is the electron-nuclear hyperfine coupling value, often expressed as a second rank tensor.

Electrically Detected Magnetoresistance and Mode of Transport

EDMR via spin-dependent trap assisted tunneling (SDTAT) was used in this work. In EDMR, the sensitivity of the response is independent of the strength of the magnetic field. In EPR, the sensitivity depends on the polarization of unpaired electron spins. In EDMR, there is an intermediate coupling of pairs of electrons which result in a sensitivity no longer strictly dependent on the polarization of unpaired electron spins, but of the permutation symmetry of the spin pair. This enables EDMR measurements at low magnetic fields and RF frequencies which would otherwise be impractical in an EPR experiment. Measuring current instead of a change in microwave power allows us to measure spin-dependent changes in the device current. In a-Si:H, we measure a spin-dependent tunneling (SDT) current. SDT currents are due to the interaction of hopping electrons with unpaired spins in defect levels distributed with in the a-Si:H. The spin-dependent nature of tunneling currents is described using a rough model based upon a seminal paper by Kaplan, Solomon and Mott (KSM) [9], which describes spin-dependent recombination current[1]. Anders et al. [10], recently showed that SDT currents can be thought of as a KSM-like interaction.

The tunneling event is forbidden between two paramagnetic sites in which the electron spin at both sites have the same spin quantum number. Electron tunneling from a defect to another, in which electrons on both sites have the same spin quantum number, is forbidden because of the Pauli Exclusion Principle. This pair of spins have a total spin angular momentum of 1 and are referred to as a triplet state. An RF resonant circuit will induce spin flipping events. When the resonance condition is satisfied and the spin flipping event takes place, the triplet state will become a singlet state (S = 0). Now that angular momentum is conserved the

[1] The KSM model was reviewed in detail by Barbanov et al. [11].

tunneling/hopping events can take place without violating the Pauli Exclusion Principle. These states are depicted below in figure 3[12].

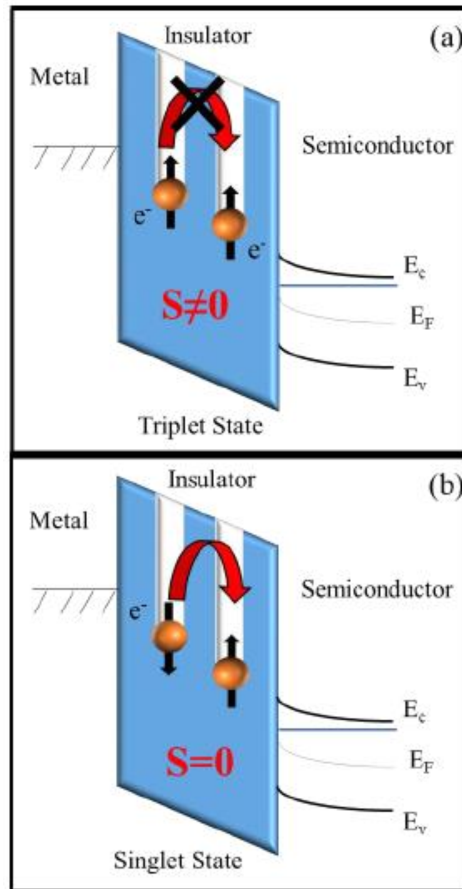

Figure 2: a) Pictorial representation of a triplet state. Electron tunneling is forbidden. b) Pictorial representation of a singlet state. Electron tunneling is permitted [13,14].

The interactions of two coupled electrons can be described via a spin Hamiltonian accounting for spin-orbit coupling, hyperfine interactions, and spin-spin interactions

$$\mathcal{H} = g\mu_B \boldsymbol{B} \cdot (\boldsymbol{S}_1 + \boldsymbol{S}_2) + \sum_i^2 \sum_j^N \boldsymbol{S}_i \cdot \boldsymbol{A}_{i,j} \cdot \boldsymbol{I}_j + J_0 \boldsymbol{S}_1 \cdot \boldsymbol{S}_2 + \boldsymbol{S}_1 \cdot \boldsymbol{D} \cdot \boldsymbol{S}_2 \quad (2)$$

where, $\mathbf{S}_1$ and $\mathbf{S}_2$ are the spin angular momentum operators for both electron spins, $\mathbf{A}_{i,j}$ is the hyperfine coupling tensor for the jth nuclei interacting with the ith electron, $\mathbf{I}_j$ is the nuclear spin angular momentum operator for the jth nuclei, J_0 is the isotropic exchange constant, and $\mathbf{D}$ is a matrix that accounts for dipole-dipole interaction between electron spins [6]. (2) can be used to gain insight about the EDMR spectra in this work.

Using an RF resonant circuit, the ratio of singlet to triplet states can be controlled [12]. When varying the ratio, the tunneling current will now change and can be measured. Hence, in SDTAT transport we can observe EDMR. SDTAT/EDMR is observed as a function of voltage across a-Si:H film. The voltage controls electron tunneling current. As bias increases, device current and EDMR amplitude will increase. The following derivation of the half-field phenomenon is presented here because it is a way to approximate spin counts using EDMR. This discussion follows the work of Slichter [6] and Cochrane et al. [8].

Since there are two electrons coupled together, there are a total of four combinations of spin angular momentum quantum numbers, $|\downarrow\downarrow\rangle$, $|\uparrow\uparrow\rangle$, $|\uparrow\downarrow\rangle$, and $|\downarrow\uparrow\rangle$. There are four allowed transitions between these four states, $|\downarrow\downarrow\rangle \leftrightarrow |\uparrow\downarrow\rangle$, $|\downarrow\downarrow\rangle \leftrightarrow |\downarrow\uparrow\rangle$, $|\uparrow\uparrow\rangle \leftrightarrow |\uparrow\downarrow\rangle$, and $|\uparrow\uparrow\rangle \leftrightarrow |\downarrow\uparrow\rangle$ [8]. The transitions from $|\downarrow\downarrow\rangle \leftrightarrow |\uparrow\uparrow\rangle$ are normally forbidden, but due to dipole-dipole interactions this

transition is allowed because the states are mixed by dipole-dipole interactions [8]. In the figure below, the energy level diagram depicting these four states and allowed transitions is shown.

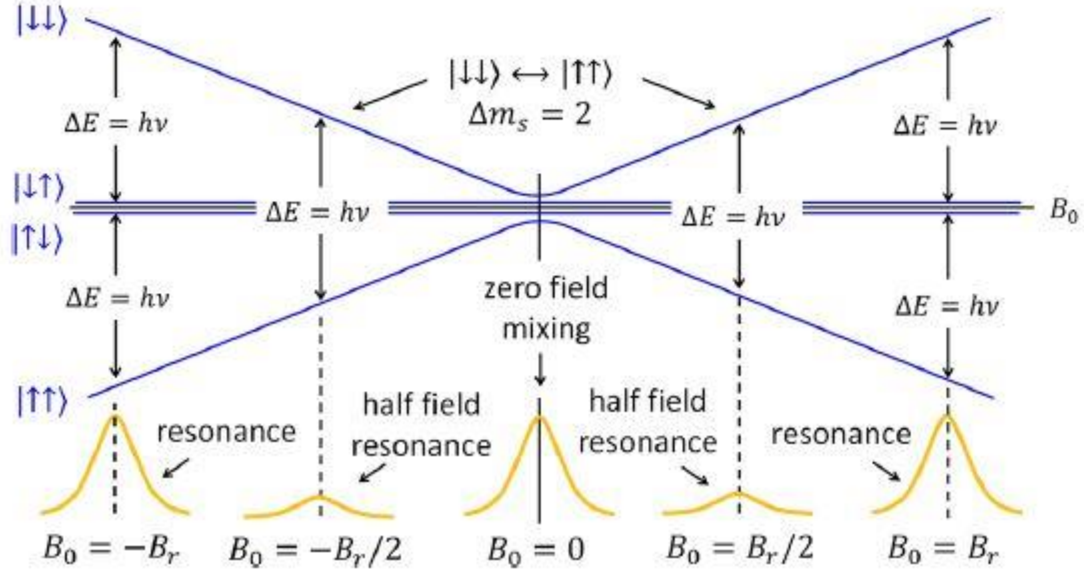

Figure 3: Energy diagram, depicting the allowed transitions between the four possible states of the coupled defects [8].

Expanding upon the dipolar term in the Hamiltonian for a-Si:H, we can rewrite the Hamiltonian as [8]

$$\widehat{H_d} = \frac{\mu_0}{4\pi}\frac{(g\mu_B)^2}{|r|^3}\left[\widehat{S_1}\cdot\widehat{S_2} - \frac{3(\widehat{S_1}\cdot r)(\widehat{S_2}\cdot r)}{|r|^2}\right] \quad (2.1)$$

where μ_0 is the permeability of free space. Recalling that the Hamiltonian multiplied by the wave function is equivalent to the energy times the wave function, the energy of the dipolar interaction can be written as follows in eq. 3.

$$E_d \approx \frac{\mu_0}{4\pi}\frac{(g\mu_B)^2}{|r|^3} \quad (3)$$

Cochrane et al. [8] showed that the ratio of the forbidden transitions to the allowed transitions is

$$R \approx \frac{4\pi}{5}\left(\frac{\mu_0}{4\pi h}\right)^2 \frac{(g\mu_B)^4}{\nu^2 {a_0}^3 {r_d}^3}, \quad (4)$$

where, R is the ratio of the integrated intensity of the half field response to the integrated intensity of the EDMR response, ν is the frequency of the RF resonant circuit, a_0 is the shortest possible distance between two defects, and r_d is the average distance between two defects. From this it is possible to determine an approximate spin count when conducting EDMR.

Near Zero Field Magneto Resistance

Near Zero Field Magneto Resistance (NZFMR) is a relatively new technique with the potential to study insulator and semiconductor-based electronics with a quite simple apparatus. NZFMR differs from EDMR in that there is no RF forcing the transitions of triplets to singlets [15]. NZFMR relies on the mixing of singlet and triplet states when the magnetic field passes through zero [16-18] (hence the name, near-zero field magnetoresistance). The big question is: Can we glean the same information from NZFMR as EDMR?

Recently, Ashton et al. compared the sensitivity of NZFMR and EDMR in radiation damaged MOSFETs [16]. In that work, planar Si/SiO_2 p-channel metal oxide semiconductor field effect transistors (MOSFETs) were subjected to ^{60}Co gamma radiation. They compared the amplitudes of the EDMR response and NZFMR response as the source/drain to body diode forward bias while maximizing the Si/SiO_2 interface recombination current via the gate bias. Since the EDMR and NZFMR responses traced in a similar manner they suggested that NZFMR has a similar physical origin as EDMR. Harmon et al. [19] also compared NZFMR and EDMR in radiation damaged MOSFETs. The more recent Harmon et al. [19] study utilized an analysis based upon the stochastic Liouville equation. Harmon et al. [19] were able to show that much of the information available in the EDMR could also be gleamed from the NZFMR.

The stochastic Liouville equation can be used to generate solutions of the density matrix. The density matrix consists of coefficients associated with possible solutions of the Schrodinger equation. Hence, the density matrix describes the statistical state of a system in quantum mechanics. Terms which become important in these solutions for the NZFMR problem are the singlet recombination rate k_s,the triplet dissociation rate k_d, and the hyperfine coupling constant. k_s is defined as the rate at which the conduction electron paired with the deep level paramagnetic defect will fall into the deep level defect, causing a recombination event with a valance band hole [19]. This will only occur if the intermediate state of the electron pair is a singlet state. k_d is the rate at which the conduction electron paired with the deep level paramagnetic defect will couple to form a triplet state and subsequently dissociate [19]. k_d and k_s along with the hyperfine coupling constants, which are the components of the hyperfine coupling tensor $\boldsymbol{A}$ from expression (2), contribute to the line shape of the NZFMR response [19].

Another system of technological importance is amorphous hydrogenated silicon nitride (a-SiN:H). In a study by Mutch et al. [12] the defects in a-SiN:H were studied via EDMR and NZFMR. Mutch et al. [12] also found that the NZFMR and EDMR were strongly correlated, indicating that they might both be useful to study SDTAT in a-SiN:H. The results were monitored with respect to voltage and temperature. If the amplitudes have similar in magnitude and line shape, that would suggest that the NZFMR technique could provide some of the information available in SDTAT. Since Harmon et al. [19] have shown that one may crudely predict the NZFMR line shape in terms of parameters already observed in EDMR, this indicates that NZFMR could have much of the analytical power of EDMR. The purpose of the following experiments is to draw parallels between the information gathered from EDMR and NZFMR using the a-Si:H semiconductor material system.

Experimental Design

A sample of 10 nm, MIS (Ti/Al – a-Si:H – p++ Si), a-Si:H was mounted on a Printed Circuit Board (PCB) T (T represents shape of the PCB). The PCB T was cleaned in ethanol and dried. A USB connector was attached to the end of the T and soldered in place. The two electrical connections were then soldered to the PCB T. The sample is attached to the PCB T electrical connection with conductive paint and then wire bonded on top to the other remaining electrical connection. The IV curve of the sample was then taken using a Hewlett-Packard Semiconductor Parameter Analyzer (HP SPA).

The EDMR spectrometer used in this study is a low-field and low-frequency spectrometer. It is comprised of a Kepco BOP 50-2M bipolar power supply, a custom built electromagnet, a Lakeshore Cyrogenics model 475 DSP Gauss meter and Hall probe, an Agilent model 83732B synthesized signal generator for RF, LabView-based digital lock-in amplifier, and Labview-based spectrometer software for magnetic field control, modulation, virtual lock-in amplification, and signal averaging. A Stanford Research Systems SR570 transimpedance preamplifier was used for biasing the device and as an analog filter. The computer was equipped with a National Instruments Data Acquisition (DAQ) Card. Below in figure 4 is a schematic diagram of the EDMR spectrometer.

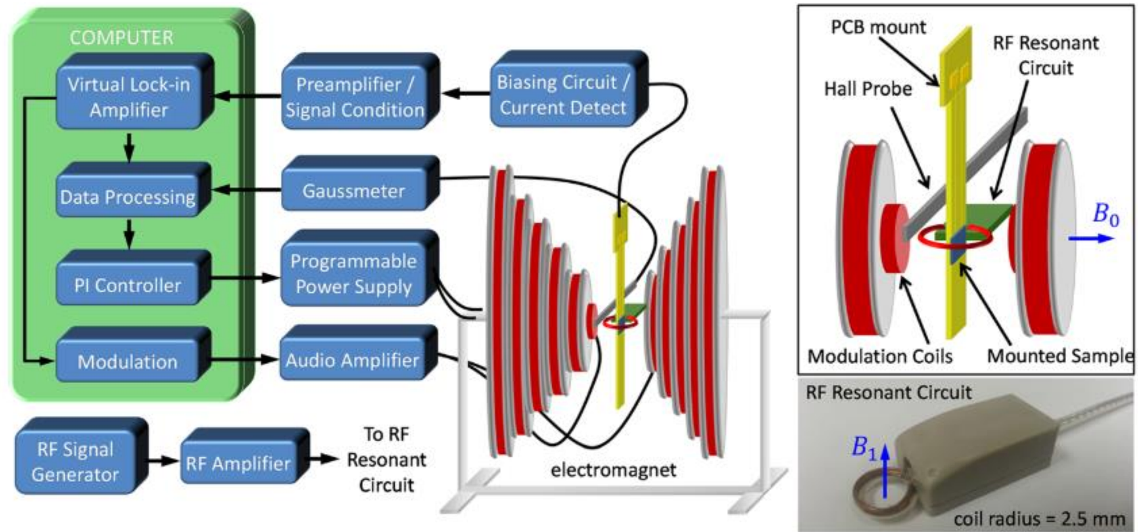

Figure 4: Low-Field apparatus for EDMR and NZFMR measurements [8]

There are many other parameters that were controlled while collecting data. In Table 1 below all parameters are listed.

Table 1: List of constant parameters during EDMR and NZFMR experiments

PARAMETER	VALUE
Sweep time (sec)	300
Center field (Gauss)	0
Sweep Width (Gauss)	200
Modulation Frequency (Hz)	1000
Modulation Amplitude (Gauss)	1
Time Constant (sec)	0.3
Temperature (K)	295
Material System	a-Si:H

Using this system, an NZFMR bias study was conducted. The voltages used were 0.25, 0.5, 0.75, 0.1, 1.1, 1.2, and 1.25 volts. To conduct NZFMR the resonant RF circuit is turned off.

Once NZFMR measurements are completed the RF coil was turned on and the measurements were run again now including both EDMR and NZFMR.

Chapter 3

Results

Because the individual scans had low signal to noise ratios (SNR), significant signal averaging was utilized in data acquisition. Processing of data was done in Matlab. At each bias, numerous scans were averaged together to create a trace. With increasing bias, the current changed drastically so the increments between voltages were shortened to show the growing EDMR/NZFMR amplitude. Finally, each trace was plotted vs. the magnetic field. Figure 5 shows both the EDMR and NZFMR responses at varying biases. Figure 6 shows the NZFMR response with the RF turned off at varying biases.

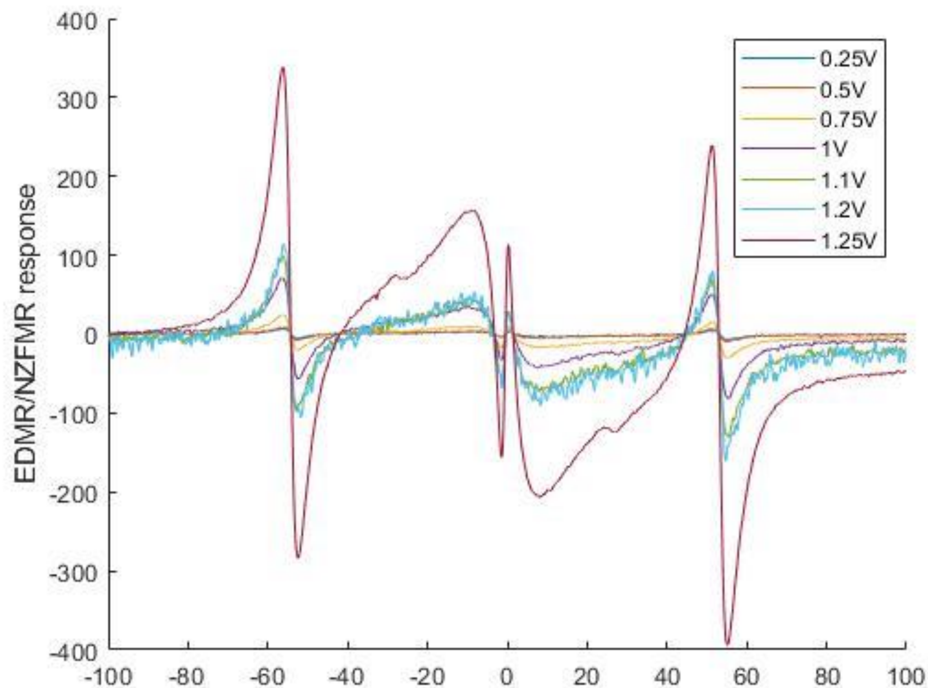

Figure 5: EDMR/NZFMR traces at varying bias in a-Si:H

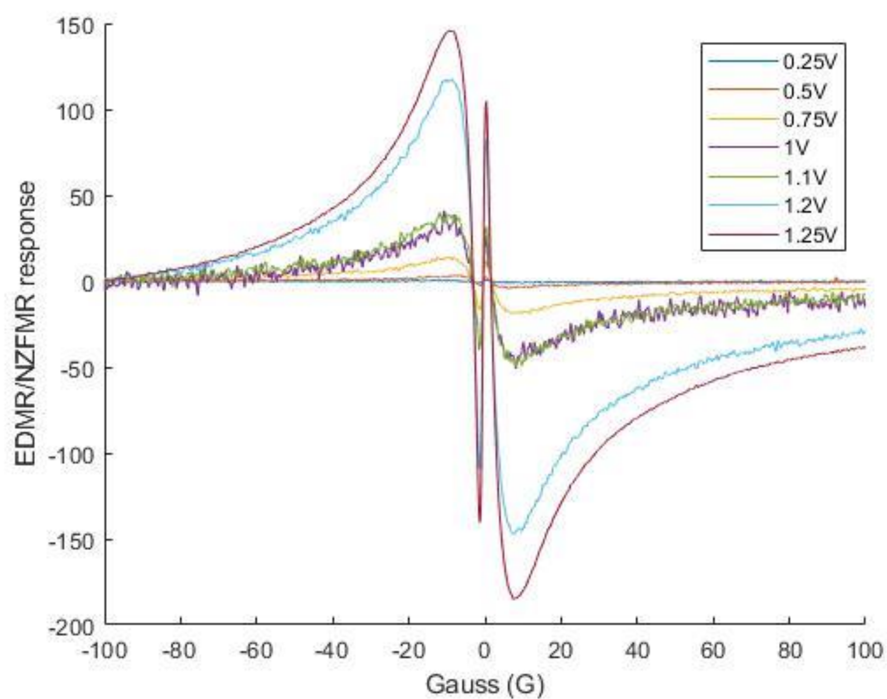

Figure 6: NZFMR traces at varying bias of a-Si:H

Chapter 4

Analysis and Conclusions

Using Matlab, the peak to peak amplitudes were measured. This amplitude was then divided by the DC current and plotted. In figure 7, I compare the amplitudes of the NZFMR response with the RF on, RF off and EDMR.

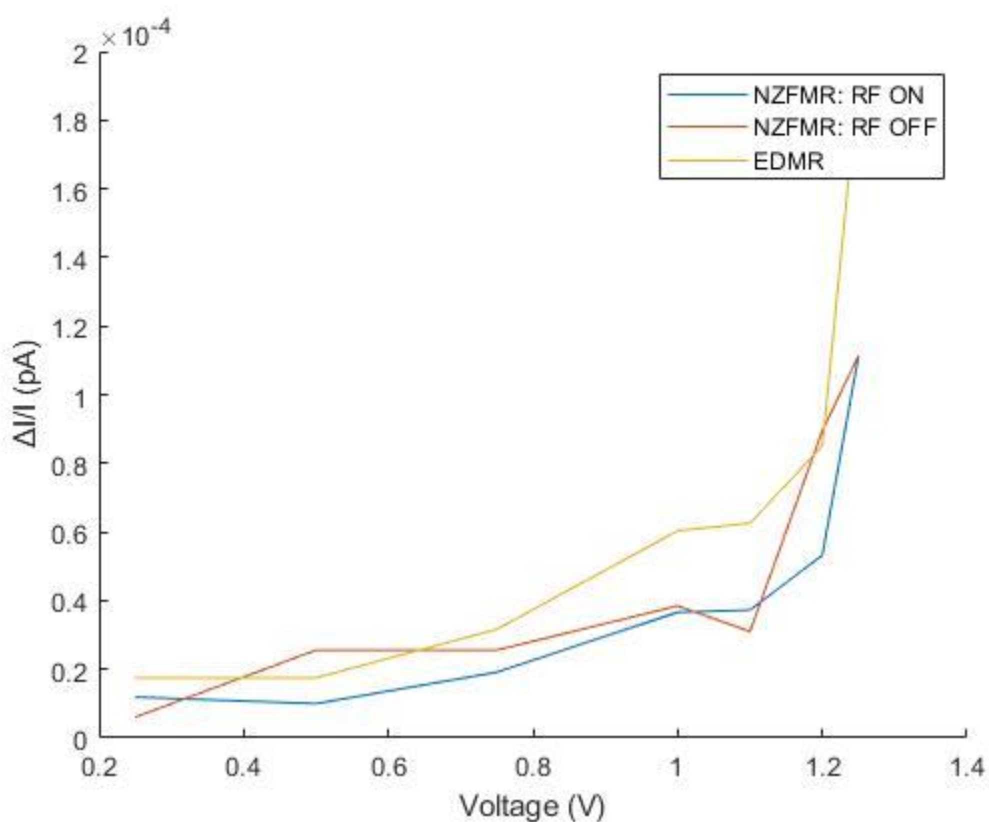

Figure 7: Amplitude the NZFMR response with the RF on, RF off and EDMR.

It is clear from figure 7, that the relative amplitude of the NZFMR with RF on is approximately equivalent to the response of NZFMR with the RF off. This shows that the NZFMR response is not dependent on the RF driving field. In a-SiN:H, Mutch et al. [12] showed that the magnetoresistance and magnetic resonance responses were quite similar with amplitudes within experimental error. This result by Mutch et al. [12] is shown in figure 8.

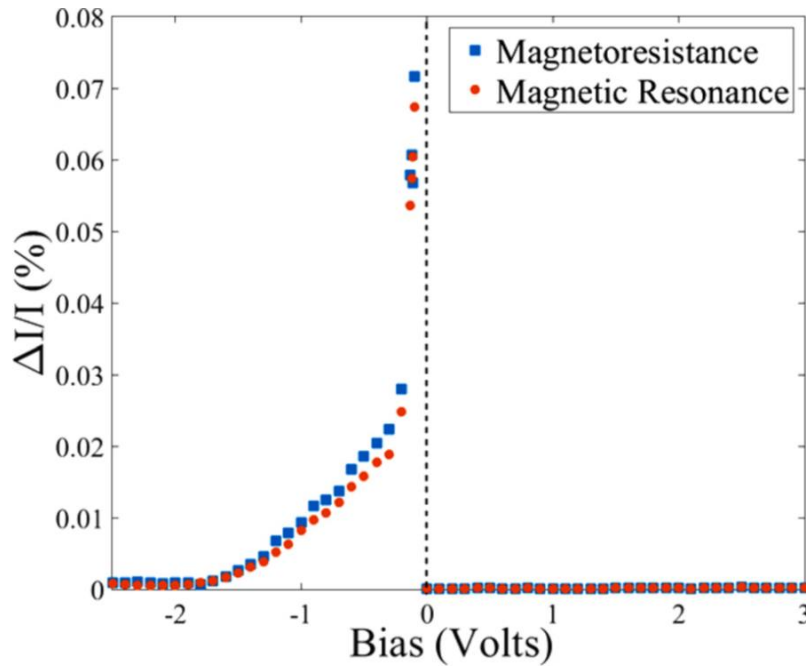

Figure 8: Results of Magnetoresistance and Magnetic Resonance amplitudes vs. bias in a-SiN:H devices [12]

This shows that EDMR and NZFMR have comparable sensitivities for studying a-Si:H. It is also notable that in this sample there is a half-field EDMR signal [20]. As shown by Cochrane et al. [8] it is possible to use half field signal to get a rough approximation for the defect density from the dipolar term of (2.1). From their work it was determined that the ratio of the integrated intensity of the half field response to the integrated intensity of the EDMR response is roughly equals 4. From (4), Cochrane et al. determined that the average distance between two defects, r_d can be expressed as in Eq. 5:

$$r_d \approx \left(\frac{6{,}937}{\upsilon^2 {a_0}^3 R}\right)^{\frac{1}{3}} \text{Å}^2 GHz^{2/3} \quad (5)$$

where, R is the ratio of the integrated intensity of the half field response to the integrated intensity of the EDMR response, ν is the frequency of the RF resonant circuit, a_0 is the shortest possible distance between two defects. In this research project, the frequency of the RF resonant circuit is 0.151 GHz, the ratio of the integrated intensities is 0.016, and the shortest distance between two defects is 4.7 Å. The shortest distance between two potential defects sites in a-Si:H was approximated to twice the bond length of crystalline Si [21]. The integrated intensity ratio was found using Matlab to analyze the half field and EDMR data taken at 1.25V. The bond length of crystalline Si is 2.35 Å [13]. Using eq. (5) the average distance between defects (r_d) is approximately 57 Å and the defect density ($1/{r_d}^3$) is about 5.4×10^{18}/cm^3. This is a rough approximation that is accurate to an order of magnitude. It is also notable that this approach for spin counting assumes that the defects are randomly distributed throughout the material, which is a reasonable approximation for a-Si:H.

Spin counts when half field responses in EDMR are present are easy to determine. Because of the complexity of the stochastic quantum Liouville solutions, we are not yet able to evaluate other parameters such as K_s and K_d [22]. Nevertheless, the similarities between the NZFMR and EDMR responses suggest that NZFMR has the capacity to explore defects within a-Si:H, with about the same sensitivity as EDMR and without the need of RF or microwave radiation. This result suggests that NZFMR may be applicable to studies of electrically active defects in 3-D integrated circuits [16,19]. While a-Si is not used in 3-D integrated circuit architecture, a-Si:H is a useful material to draw connection between the NZFRM and EDMR due to the strong response from both phenomena and simplified defect structure.

There is a plethora of information which can be gleamed from low-field EDMR. Of particular interest is a rough approximation of the defect density, if a half-field response is present

[19,20]. In principle, using the linewidth and shape of the zero-field response, information can be gained about k_d and k_s. With yet another material system in which the NZFMR sensitivity is comparable to EDMR, the group of materials in which the NZFMR and EDMR sensitivities are comparable has expanded.

References

[1] I. M. P. Aarts *et al*, "Absolute in situ measurement of surface dangling bonds during a-Si:H growth," *Applied Physics Letters,* vol. 90, *(16),* pp. 161918-1/3, 2007.

[2] B. Kuyken *et al*, "On-chip parametric amplification with 26.5 dB gain at telecommunication wavelengths using CMOS-compatible hydrogenated amorphous silicon waveguides," *Optics Letters,* vol. 36, *(4),* pp. 552, 2011.

[3] S. K. Selvaraja *et al*, "Low-loss amorphous silicon-on-insulator technology for photonic integrated circuitry," *Optics Communications,* vol. 282, *(9),* pp. 1767-1770, 2009.

[4] S. De Wolf, S. Olibet and C. Ballif, "Stretched-exponential a - Si : H ⁄ c - Si interface recombination decay," *Applied Physics Letters,* vol. 93, *(3),* pp. 032101-032101-3, 2008.

[5] J. Zhu *et al*, "Optical Absorption Enhancement in Amorphous Silicon Nanowire and Nanocone Arrays," *Nano Letters,* vol. 9, *(1),* pp. 279-282, 2009.

[6] C. P. Slichter, Principles of Magnetic Resonance. (3rd enl. and updat ed.) New York;Berlin;: Springer-Verlag, 1990.

[7] J. A. Weil, J. R. Bolton and Wiley InterScience (Online service), *Electron Paramagnetic Resonance: Elementary Theory and Practical Applications.* (2nd ed.) 2007.

[8] C. J. Cochrane and P. M. Lenahan, "Spin counting in electrically detected magnetic resonance via low-field defect state mixing," *Applied Physics Letters,* vol. 104, *(9),* pp. 93503, 2014.

[9] *D. Kaplan, I. Solomon, N.F. Mott. Explanation of the large spin-dependent recombination effect in semiconductors. Journal de Physique Lettres, 1978, 39 (4), pp.51-54. <10.1051/jphyslet:0197800390405100>. <jpa-00231440>*

[10] M. A. Anders *et al*, "Physical nature of electrically detected magnetic resonance through spin dependent trap assisted tunneling in insulators," *Journal of Applied Physics,* vol. 124, *(21),* pp. 215105, 2018.

[11] A. Barabanov, O. Tretiak and V. L'vov, "Complete theoretical analysis of the Kaplan-Solomon-Mott mechanism of spin-dependent recombination in semiconductors," *Physical Review. B, Condensed Matter,* vol. 54, *(4),* pp. 2571-2577, 1996.

[12] M. J. Mutch, P. M. Lenahan and S. W. King, "Defect chemistry and electronic transport in low-κ dielectrics studied with electrically detected magnetic resonance," *Journal of Applied Physics,* vol. 119, *(9),* pp. 94102, 2016.

[13] W. Wagemans and B. Koopmans, "Spin transport and magnetoresistance in organic semiconductors," *Physica Status Solidi (B) Basic Research,* vol. 248, *(5),* pp. 1029-1041, 2011.

[14] M. J. Mutch, P. M. Lenahan and S. W. King, "Spin transport, magnetoresistance, and electrically detected magnetic resonance in amorphous hydrogenated silicon nitride," *Applied Physics Letters,* vol. 109, *(6),* pp. 62403, 2016.

[15] S. J. Moxim *et al*, "Observation of Radiation-Induced Leakage Current Defects in MOS Oxides With Multifrequency Electrically Detected Magnetic Resonance and Near-Zero-Field Magnetoresistance," *IEEE Transactions on Nuclear Science,* vol. 67, *(1),* pp. 228-233, 2020.

[16] J. P. Ashton *et al*, "A New Analytical Tool for the Study of Radiation Effects in 3-D Integrated Circuits: Near-Zero Field Magnetoresistance Spectroscopy," *IEEE Transactions on Nuclear Science,* vol. 66, *(1),* pp. 428-436, 2019.

[17] N. J. Harmon and M. E. Flatté, "Spin-flip induced magnetoresistance in positionally disordered organic solids," *Physical Review Letters,* vol. 108, *(18),* pp. 186602, 2011.

[18] N. J. Harmon and M. E. Flatté, "Semiclassical theory of magnetoresistance in positionally disordered organic semiconductors," *Physical Review B,* vol. 85, *(7),* 2012.

[19] N. J. Harmon *et al*, "Modeling of Near Zero-Field Magnetoresistance and Electrically Detected Magnetic Resonance in Irradiated Si/SiO2 MOSFETs," *IEEE Transactions on Nuclear Science,* pp. 1-1, 2020.

[20] S. S. Eaton *et al*, "Use of the ESR half-field transition to determine the interspin distance and the orientation of the interspin vector in systems with two unpaired electrons," *Journal of the American Chemical Society,* vol. 105, *(22),* pp. 6560-6567, 1983.

[21] A. V. Shah *et al*, "Thin-film silicon solar cell technology," *Progress in Photovoltaics: Research and Applications,* vol. 12, *(2-3),* pp. 113-142, 2004.

[22] F. C. Rong *et al*, "Spin-dependent Shockley-read recombination of electrons and holes in indirect-band-gap semiconductor p- n junction diodes," *Solid State Electronics,* vol. 34, *(8),* pp. 835-841, 1991